

# HDR Environment Map Estimation with Latent Diffusion Models

Jack Hilliard

jh00695@surrey.ac.uk

Adrian Hilton

a.hilton@surrey.ac.uk

Jean-Yves Guillemaut

j.guillemaut@surrey.ac.uk

University of Surrey

## Abstract

We advance the field of HDR environment map estimation from a single-view image by establishing a novel approach leveraging the Latent Diffusion Model (LDM) to produce high-quality environment maps that can plausibly light mirror-reflective surfaces. A common issue when using the ERP representation, the format used by the vast majority of approaches, is distortions at the poles and a seam at the sides of the environment map. We remove the border seam artefact by proposing an ERP convolutional padding in the latent autoencoder. Additionally, we investigate whether adapting the diffusion network architecture to the ERP format can improve the quality and accuracy of the estimated environment map by proposing a panoramically-adapted Diffusion Transformer architecture. Our proposed PanoDiT network reduces ERP distortions and artefacts, but at the cost of image quality and plausibility. We evaluate with standard benchmarks to demonstrate that our models estimate high-quality environment maps that perform competitively with state-of-the-art approaches in both image quality and lighting accuracy.

## 1. Introduction

The research on illumination estimation from a Limited Field of View (LFOV) Low Dynamic Range Image (LDRI) for Image-Based Lighting (IBL) has followed the trends in image generation to improve the quality of the estimated environment maps. Image quality is crucial when using environment maps to light mirror reflective surfaces, as the details in the environment map will be visible on the rendered surface. Consequently, any image artefacts or implausibility in the estimated environment map will reduce the plausibility of the composited object. Trends in image generation [12, 13, 27, 49, 60] have often been adopted in the field of illumination estimation to improve environment map generation [2, 10, 26, 46]. Recent image generation models have used Latent Diffusion Model (LDM)s to great effect; Latent Diffusion, proposed by Rombach *et al.* [37], and Sta-



Figure 1. Examples of objects with different surface properties rendered with indoor (*top*) and outdoor (*bottom*) HDR environment maps generated from our LDM with U-Net backbone.

ble Diffusion [14, 36, 38] can both produce images nearly indistinguishable from those captured with a camera or created by an artist. These models have consistently proven their adaptability to different tasks, including the field of inpainting and outpainting [30, 33, 36–38, 52, 53].

The standard image format for IBL illumination estimation is the 360° Equirectangular Panorama (ERP) image as it contains the illumination conditions for the whole scene at the camera position in a single image [2, 5, 10, 16, 17, 40, 41, 50, 58]. Various approaches have been proposed to adapt neural networks to the ERP image format and can be categorised as image manipulations at inference, loss function tailoring or architecture adaptations. A few models have been proposed for applying LDMs to ERP image generation [5, 32, 47, 52], however, they have not adapted the Denoising Diffusion Probabilistic Model (DDPM) architecture to ERPs as they use foundational models that prevent

this. Consequently, ERP artefacts have not been removed or inference time and memory requirements have increased.

We present an LDM that estimates the High Dynamic Range (HDR) environment map, which can be used for IBL, from an LFOV LDRI and its associated LFOV mask in ERP format. It works at a resolution of 256 by 512 for both indoor and outdoor environments. For the Latent Autoencoder (LAE), we propose an ERP convolutional padding that removes the border seam introduced when encoding and decoding an ERP image. Additionally, we propose two variations of the model: one with the DDPM U-Net of [37], the other, a panoramically adapted Diffusion Transformer (DiT), PanoDiT, that uses a Diffusion Pitch Attention Module (DPAM) that employs the PAM from PanoSWIN [31] to improve the network’s understanding of the ERP representation.

We evaluate each model’s ability to remove ERP artefacts by observing rotated panoramas and cube-map representations to compare the common locations where ERP artefacts and warping occur. We quantitatively compare using standard illumination estimation benchmarks proposed by Weber *et al.* [50]. Through this evaluation, we demonstrate that both our models perform competitively with state-of-the-art approaches. We also note that the DDPM with U-Net architecture produces environment maps with better image quality and the PanoDiT architecture estimates lighting more accurately. Furthermore, we compare against current state-of-the-art illumination estimation methods to demonstrate the ability of our models. Examples of rendered objects with our environment maps are presented in Figure 1. Our contributions are summarised as follows:

- To the author’s knowledge, this work is the first implementation of an LDM to the task of HDR environment map estimation from an LFOV LDRI in ERP image format.
- We present a novel convolutional padding and DDPM architecture designed for the ERP image format. These remove the border seam and homogenise generation at the sides of the image, creating a continuous panorama.
- We evaluate our models with standard benchmarks to demonstrate that they perform at a state-of-the-art level, reducing the ERP artefacts and accurately rendering diffuse, glossy and mirror reflective surfaces.

## 2. Related Work

**Illumination Estimation** The field of illumination estimation from a single-view image is a long-standing field of computer vision and neural rendering. This field aims to estimate the full 360° lighting conditions of a scene at the point of the camera’s location from a single LFOV LDRI. Classically, this was achieved by photographing

multiple light probes of different surface reflectance properties from different angles and stitching the captured images into a 360° ERP environment map [11]. However, this approach is not viable for real-time rendering applications such as Mixed Reality (MR) object compositing. The seminal work of Gardner *et al.* [16] first proposed the use of a Convolutional Neural Network (CNN) autoencoder to estimate the HDR environment map of a scene from a single LDRI. Recent illumination estimation works have opted for an IBL approach [2, 10, 16, 22, 23, 26, 40, 41, 46, 50, 58] over a basis function regression [3, 6, 17–19, 24, 25, 29, 55–57, 59] as the HDR environment maps used in IBL contain the detail required to render mirror reflective objects with features from the scene appearing on their surface. To further enhance the plausibility of the environment map for rendering mirror-reflective objects, there has been a focus on improving image quality by utilising state-of-the-art models from the field of image generation. StyleLight [46] used a modified StyleGANv2 [27], Akimoto *et al.* [2] implemented a VQGAN [13], Hilliard *et al.* [22] proposed a U-Net style Vision Transformer (ViT) [12, 49] and EverLight [10] and ImmerseGAN [26] a modified version of the CoModGAN [60].

We leverage the current state-of-the-art in image generation architecture, the LDM, to further advance the field of illumination estimation and improve the image quality using a smaller training dataset than the current state-of-the-art.

**Latent Diffusion Models** LDMs [37] have proven to produce realistic images with a large variation in their semantic distribution and have since been adapted and applied to various computer vision applications including image inpainting and outpainting by [30, 33, 36–38, 52, 53]. Stable Diffusion models [36, 38] use the mask and encoded masked image as the condition of the denoising process through a hybrid method of concatenation at the beginning of each denoising step and cross-attention throughout the DDPM. LDMs have also been applied to generate and manipulate 360° ERPs [32, 47, 52]. StitchDiffusion [47] adopts the MultiDiffusion model to customise 360° panoramas with text prompts. AOG-Net [32] outpaints 360° ERPs from an LFOV image by progressively outpainting a local region in an autoregressive manner. Each local region is outpainted with an LDM backbone [37] using a text prompt, global cubemap, spherical geometry cubemap projection and the LFOV to be outpainted. PanoDiffusion [52] builds on [37] to outpaint both the RGB and depth map in 360° ERP from an LFOV RGB input image. Although both [47] and [52] design their methods for ERP images, they do not completely remove the border seam artefact.

**Adapting Deep Learning Models to 360° ERP** 360° ERPs are spherical surfaces warped to be presented on a 2D plane and, as such, represent the illumination conditions at a point in a scene in image format. However, this for-



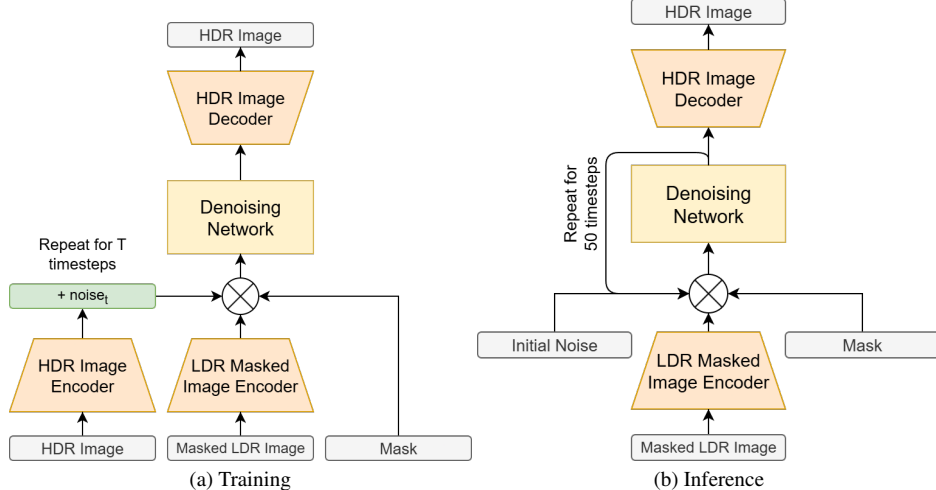


Figure 2. Summary of the training and inference processes. During training, the model applies noise to the latent HDR Image at each timestep. During inference, random noise is used as the initial input to the model and concatenated with the conditions. At each successive timestep, the output of the Denoising Network is used in place of the initial noise.

mat incurs warped areas at the top and bottom of the image and includes the consideration that the sides of the image are connected. When using this format in neural networks, artefacts can often appear where objects are not correctly generated at the poles of the image and the sides are not homogeneously generated, often with a seam at the border. Solutions to remove these artefacts generated by deep learning models can be put into three categories: image manipulations [1, 2, 7, 10, 15, 20, 21, 23, 28, 30, 40, 47, 52, 54], tailoring loss functions [2, 10, 26, 40] and adapting architectures [8, 9, 22, 39, 43, 44, 56].

Adapting the neural network architecture has proven advantageous as it removes the need for the network to learn the warped formatting. These adaptations can remove border seams and warping at the poles with the added benefits of higher-quality image generation. Initial approaches adapted the kernel shape of convolutional neural networks [8, 9, 43–45]. Later adaptations were applied to the ViT architecture. PanoFormer [39] adapted a ViT attention block with a panoramic structure-guided transformer block. Attention was performed between a central token and 8 surrounding tokens to prevent warping. This adopted a UFormer [49] style architecture with circular padding for horizontal sides during convolutions. Ling *et al.* [31] observed that attention windows at the poles of the ERP should be considered connected. They proposed PanoSWIN, which changed the shifted window attention layout to account for the connections at the ERP borders and implemented a pitch attention module to further account for the ERP warping at the poles.

Currently, in the field of illumination estimation, only EMLight [56] and 360U-Former [22] have adapted the

model architecture to the ERP representation. We compare the use of the pitch attention module in a DiT against a standard U-Net to compare how adapting the DDPM architecture affects the quality of the generated environment map. Furthermore, we explore the use of adapted convolutional layers in the LAE to remove ERP border artefacts, which are present in the majority of illumination estimation approaches.

### 3. Methodology

We propose a novel method to estimate the HDR environment map of a scene, at the camera position, from an LFOV LDRI building on the LDM design of Rombach *et al.* [37] and masked outpainting approach of [36, 38]. Furthermore, we propose two crucial modifications to the model architecture to remove and reduce artefacts caused by the ERP image format. We first give an overview of our LDM, detailing the structure, training and inference processes. We then discuss the role of the LAE and our developments to remove the ERP border seam. Finally, we describe the function of the DDPM and our proposed PanoDiT that reduces the ERP distortions.

#### 3.1. Model Overview

The LDM consists of two core components: the LAE and the DDPM. The model’s training is two-fold: first, Low Dynamic Range (LDR) and HDR autoencoders are trained to encode and decode an image into and out of latent space. Second, the model learns to denoise an encoded High Dynamic Range Image (HDRI) with added noise, given an encoded LFOV LDRI and a mask. Noise is incrementally dif-



Figure 3. The ERP padding we use in our convolutions of the LAE. Our network uses a padding of 1 during convolutions, here we choose a padding of 8 so it can be visualised.

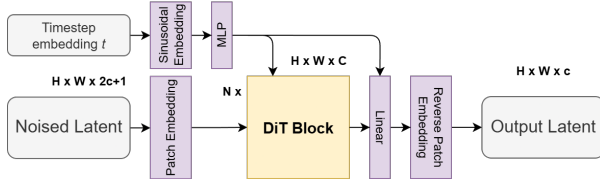


Figure 4. The DiT network diagram. The input is the concatenated mask, the latent space masked image and the latent space noisy image. The output is the denoised latent space image.

fused onto the encoded HDRI and the network is trained to learn the previous step in the diffusion process. During inference, the model iteratively denoises random noise so that it can infer the most likely ERP HDR environment map, given the encoded LFOV LDRI and mask as conditions. The overall pipeline for training and inference can be seen in Figure 2.

### 3.2. Latent Autoencoder

The LAE, composed of an encoder  $\varepsilon(\cdot)$  and decoder  $D(\cdot)$ , encodes an image  $x_0$  into latent space  $z_0 = \varepsilon(x_0)$  and reconstructs it from this latent dimension  $x_0 = D(z_0)$ . We use two LAEs in our model, one for LDRI  $\varepsilon_L$  and the other for HDRI  $\varepsilon_H$ . We use the Kullback Leibler (KL) divergence autoencoder, as suggested by Esser *et al.* [14]. Our autoencoders encode images of resolution 256x512x3 to a latent space of 32x64x4. We found that this scale is most appropriate, as the Field of View (FOV) masks would dramatically warp and become misaligned due to interpolation errors at lower resolution scales. We adapt our autoencoder to understand the border adjacency of ERP images by implementing an ERP padding instead of the standard convolutional padding. Our ERP padding, Figure 3, combines circular padding at the sides of the image with a flipped mirror padding at the top and bottom to account for the adjacent pixels at the poles of ERP. This form of convolutional padding allows our autoencoders to recreate images without border seams.

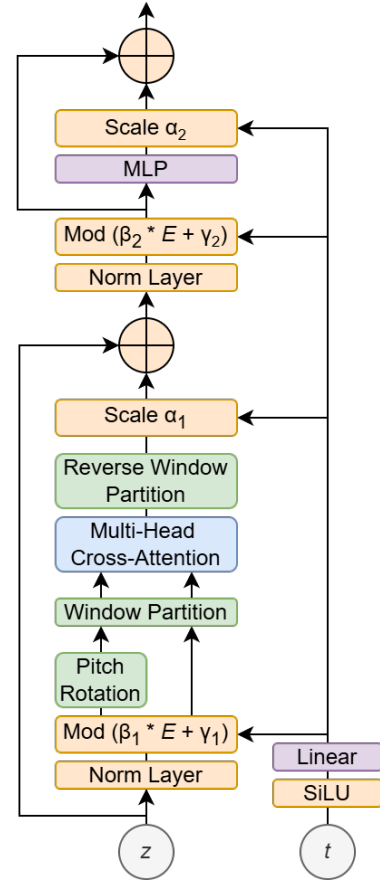


Figure 5. DPAM block diagram with added timestep embedding.

### 3.3. Denoising Diffusion Probabilistic Model

The DDPM  $\epsilon_\theta$  learns to predict the next step in the inverse distribution given the noisy latent  $z_t$  and encoded conditions  $z_L$  and mask  $m$

$$\epsilon_\theta(z_t, t, z_L, m) = (z_t - \bar{\alpha}_t z_\theta(z_t, t)), \quad (1)$$

where  $z_\theta$  is the estimated starting latent based on the current step  $z_t$ . The noisy latent  $z_t$  is produced by adding noise in

a Markovian manner

$$q(z_t|z_0) = \mathcal{N}(z_t; \sqrt{\bar{\alpha}_t}z_0, (1 - \bar{\alpha}_t)\mathbf{I}), \quad (2)$$

and the constant  $\bar{\alpha}_t$  is a hyperparameter. The overall model can be defined as:

$$L_{LDM} := \mathbb{E}_{\varepsilon_H(x), z_L, m, \epsilon \sim \mathcal{N}(0,1), t} [\| \epsilon - \epsilon_\theta(z_t, z_L, m, t) \|_2^2]. \quad (3)$$

For the U-Net DDPM network, we use the configuration from [37]. Furthermore, we propose PanoDiT, a DiT style architecture [34] that consists of a series of ViT blocks with additional timestep embedding and can be seen in Figure 4. The purpose of PanoDiT is to reduce the distortions caused by representing the 360° lighting conditions of a scene at a point on a 2D ERP image. To create a network that understands the distortions that occur in the ERP format, we introduce a Diffusion Pitch Attention Module (DPAM) that combines timestep embedding with the PAM from PanoSWIN [31]. We implement the timestep embedding using a shared adaLN-single parameter [35], in line with [5, 14, 34]. The PAM applies a window partition to the ERP image and performs cross-attention between each window with the respective window from the ERP rotated and pitched by 90°. This allows the network to understand the relationship between objects at different positions in the ERP. The DPAM is presented in Figure 5. The PanoDiT consists of 21 DiT blocks with 16 attention heads and a hidden dimension size of 1024. We use the PAM every 7th block, 3 times in total.

## 4. Evaluation

We compare our models against state-of-the-art illumination estimation methods, the results of which have been generously contributed to the community by Karimi *et al.* [10] and can be found on the EverLight project website<sup>1</sup>. Next, we conduct an ablation study on the LAE to demonstrate the effectiveness of our ERP convolutional padding. An ablation study is not performed on the DDPM networks as we evaluate both models when comparing against other illumination estimation methods. Additional results are included in the supplementary material.

### 4.1. Implementation Details

All networks are trained on indoor and outdoor data at an image resolution of 256x512. For the indoor data, we use the Structured3D [61] synthetic dataset which contains 21,843 photo-realistic ERPs. For the outdoor data, we use the 360 Sun Positions [4] dataset which contains 19,093 360° street view images of both urban roads and rural environments. We generate the HDR pairs for both datasets using the LDR-to-HDR network from [22]. We augment both

datasets by horizontally rotating each panorama 4 times randomly between 60° and 285° at intervals of 45° with a 20% chance of being horizontally flipped for a total of 204,680 images. When training our LDR autoencoder, we randomly mask 50% of the panoramas with a random LFOV mask so that it can be used for both LDR ERPs and LFOV LDRI. We split each augmented dataset into a train/test ratio of 99:1 and ensure that all augmented versions of each pair exist only in the train or the test subset to prevent overfitting. Each DDPM architecture is trained on a range of randomly chosen LFOV sizes {40°, 60°, 90°, 120°} for the masked input. Each latent autoencoder is fine-tuned for 30 epochs on 2 NVIDIA A100 GPUs with ADAM optimiser with a learning rate of  $4.5 \times 10^{-6}$  and betas 0.5 and 0.9. The LDR autoencoder is fine-tuned from the f=8, KL autoencoder provided by [37]. The HDR autoencoder is fine-tuned on our LDR autoencoder. Both DDPMs are trained from scratch for 50 epochs on an A100 NVIDIA GPU with the AdamW optimiser with a learning rate of  $2.0 \times 10^{-6}$ . We train our DDPM with 1000 timesteps and use 50 for inference.

### 4.2. Comparison with Illumination Estimation Methods

This comparison is split into indoor and outdoor scene domains, as the majority of previous methods are designed for either domain and each evaluation uses different datasets. For each domain, we compare quantitatively and qualitatively. For the quantitative measurements, Table 1, we compare semantic similarity and diffuse light position and colour accuracy [50]. For our qualitative comparisons, we visually compare key locations of the generated ERPs to identify potential artefacts and assess the quality at these areas. We present environment maps horizontally rotated by 180° to observe potential border seams or discontinuous generation. The top and bottom faces of the cube map representation are used to identify distortions at the poles.

#### 4.2.1 Indoor Scenes

For indoor scenes, we follow the two-fold evaluation protocol of [50]: first, the generated environment maps are used to light a scene with 9 diffuse spheres on a ground plane. This measures the ability of each model to produce accurate light positions, colours and intensities on a diffuse surface. Second, the plausibility of the generated HDRI is measured with Fréchet Inception Distance (FID) score. The rendering tests use the 224 images from the test split of the Laval HDR Indoor dataset [16]. The FID score uses the 305 images from the Laval HDR Indoor test set [16] and the 192 indoor images from [6]. Additional datasets help to remove the potential bias of using a single dataset. For each metric, we extract 10 views of 50° for each image.

<sup>1</sup><https://lvsn.github.io/everlight/>

Method	si-RMSE↓	RMSE↓	RGB ang.↓	PSNR↑	FID↓
INDOOR METHODS					
Ours <sub>U-Net</sub>	0.048	<u>0.091</u>	11.13°	<u>12.98</u>	<u>64.31</u>
Ours <sub>PanoDiT</sub>	<u>0.046</u>	<b>0.085</b>	10.78°	<b>13.49</b>	83.49
360U-Former[22]	<b>0.033</b>	0.110	6.11°	11.68	119.91
EverLight[10]	0.087	0.239	5.75°	10.04	65.50
Weber’22[50]	0.079	0.196	<u>4.08°</u>	12.95	130.13
EMLight[56]	0.099	0.232	<b>3.99°</b>	10.34	135.97
ImmerseGAN[26]	0.091	0.215	7.89°	10.87	<b>55.46</b>
OUTDOOR METHODS					
Ours <sub>U-Net</sub>	<u>0.052</u>	<u>0.152</u>	<u>5.44°</u>	11.23	83.17
Ours <sub>PanoDiT</sub>	<u>0.052</u>	<b>0.135</b>	5.62°	<u>12.44</u>	90.74
360U-Former[22]	<b>0.049</b>	0.161	<b>4.00°</b>	<b>13.27</b>	102.63
EverLight[10]	0.162	0.385	8.30°	11.01	<u>61.49</u>
ImmerseGAN[26]	0.175	0.341	9.56°	10.91	<b>34.43</b>

Table 1. Indoor and outdoor quantitative comparison with various illumination estimation methods. The metrics si-RMSE, RMSE, RGB ang. and PSNR are evaluated by rendering a diffuse scene. The FID score is calculated on the generated environment maps. The **best** and second-best scores for each metric and domain are highlighted.

The FID score of our U-Net model outperforms all models by a noticeable margin, except for EverLight and ImmerseGAN. This is supported by our environment maps, presented in Figure 6, which show more complex and detailed scenes with greater variance than 360U-Former and Weber *et al.* In terms of ERP artefacts, our U-Net and PanoDiT LDMs and the 360U-Former do not introduce the border seam that is visible in [50] and subtly perceptible in EverLight. When comparing generations at the poles, all models produce an unrealistic shadowing effect, a result of a light source generated on one side of the panorama and not on the other. This pinching effect is subtly present in our PanoDiT model, proving that the DPAM can reduce ERP artefacts at the poles. In terms of lighting accuracy, our PanoDiT model performs at state-of-the-art level at estimating the colours of the light sources, measured by si-RMSE, RMSE and PSNR. However, the RGB angular error is particularly poor for indoor scenes.

#### 4.2.2 Outdoor Scenes

For outdoor scenes, the quantitative comparison is conducted similarly to the indoor scenes, the input is changed to 3 perspective crops at azimuth spacing  $\{0, 120, 240\}$  of 90° FOV. We use the 893 outdoor panoramas from the [6] dataset, totalling 2,517 images for evaluation. We compare our approach with the works of Everlight [10], ImmerseGAN [26] and 360U-Former [22].

The results in Table 1 show that our approaches outperform EverLight and ImmerseGAN and are competitive with 360U-Former in terms of RMSE and si-RMSE. When

observing the environment maps in Figure 6, our models consistently and correctly estimate the sun position and the amount of cloud cover. Supported by the FID score, our method can generate realistic features and textures compared to the 360U-Former. However, EverLight and ImmerseGAN continue to outperform our approach, potentially due to training on a larger dataset. In terms of lighting accuracy, the PanoDiT model outperforms the U-Net. Additionally, there is a stronger correlation towards PanoDiT on the indoor datasets, which have more complex lighting with multiple sources to estimate. This could suggest that an inherent understanding of the ERP warping could assist in accurate light positioning.

#### 4.2.3 DDPM Comparison

The quantitative results in Table 1 show that the U-Net, despite being a smaller and less complex model, can generate more plausible and higher-quality images than the PanoDiT. Whereas the PanoDiT more accurately estimates the lighting conditions. Comparing the panoramas in Figure 6, the U-Net produces panoramas that have fewer artefacts, while generated objects and features appear familiar. The PanoDiT tends to produce abstract features and textures. However, the warping at the poles of the ERP is reduced compared to the U-Net.

For both models, we occasionally observe that the generated scene does not semantically or contextually match that of the ground truth. For indoor scenes, we often notice living spaces and bathrooms being generated. For outdoor scenes, a rural space may be generated as an urban space



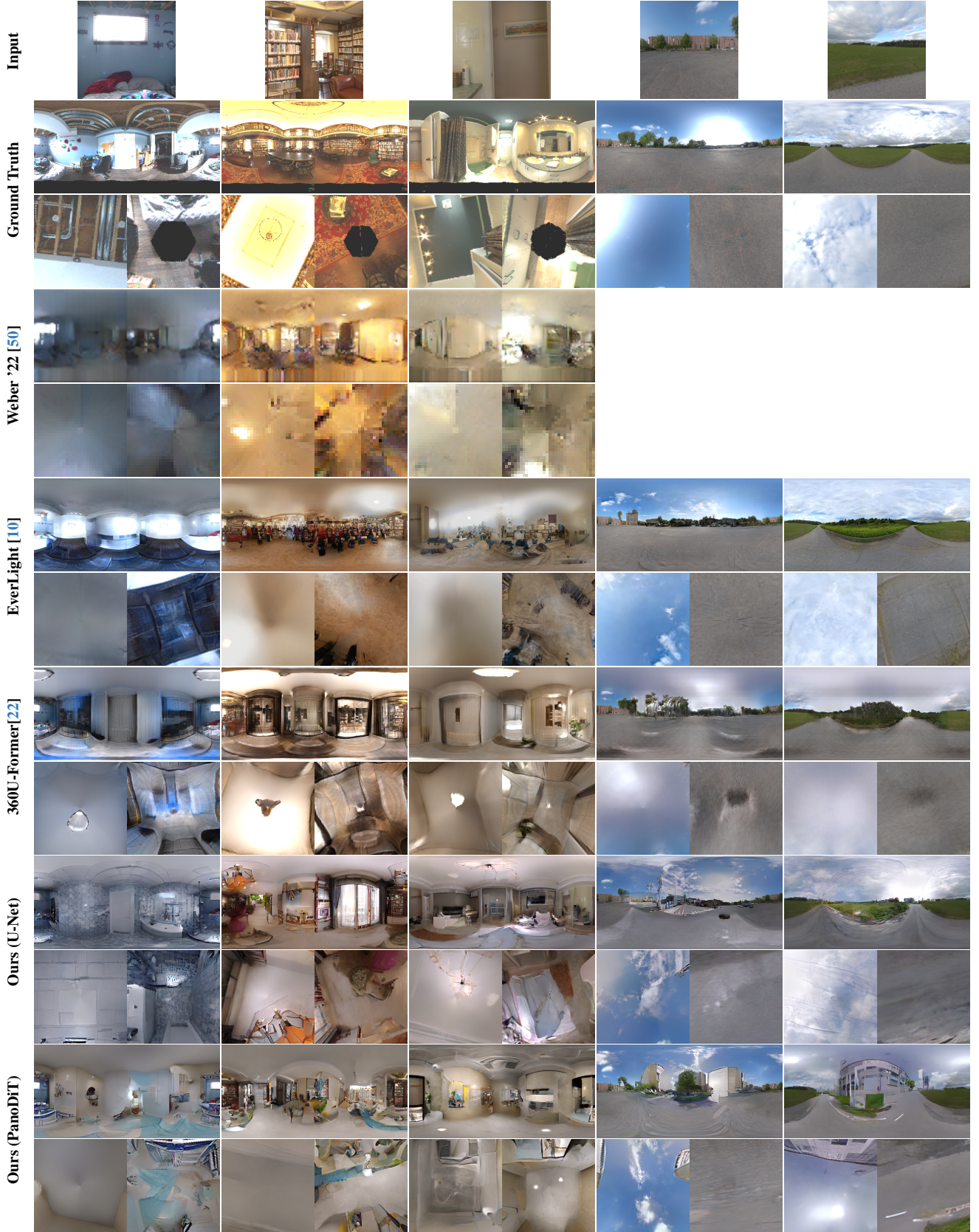


Figure 6. Indoor qualitative comparison of our method with state-of-the-art methods. For each method and input LFOV image, we show the ERP rotated 180°, to show potential border seams, and the top and bottom cube map faces, to visualise generation at the poles.

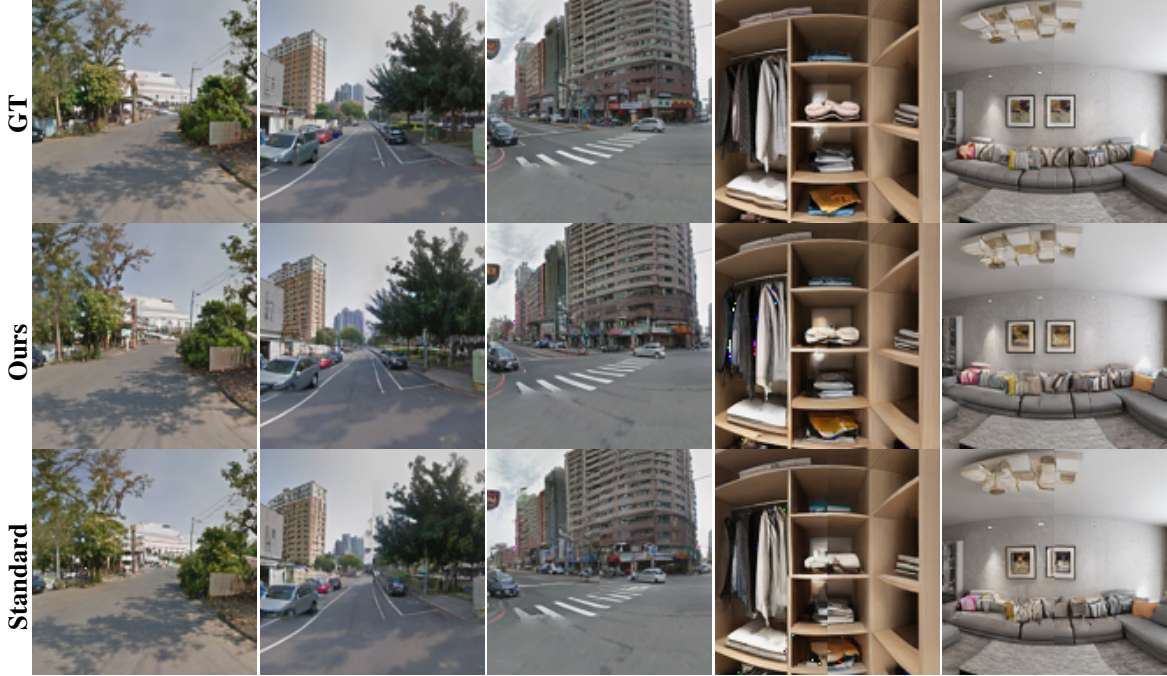


Figure 7. Comparison of the LDR ERPs recreated by the LAE with and without our ERP padding. A crop is taken from the centre of the panoramas to view the border seam.

	si-RMSE↓	RMSE↓	SSIM↑	PSNR↑	FID↓
ERP Convolutional Padding	<b>0.04155</b>	<b>0.04155</b>	<b>0.8953</b>	<b>28.04</b>	7.62
Standard Convolutional Padding	0.04331	0.04335	0.8896	27.60	<b>7.61</b>

Table 2. A quantitative comparison of our LAE’s ability to reconstruct an LDR ERP against an LAE with standard convolutional padding. The best results are highlighted in **bold**.

and vice versa. A severe case of this occurs when a scene will be generated as indoor when the ground truth is outdoor and vice versa. These problems are likely a consequence of training on limited datasets, with only a small variance in scene type.

### 4.3. Latent Autoencoder Ablation

In Figure 7, we demonstrate the ability of our proposed ERP convolutional padding against standard convolutional padding to remove border seam artefact by comparing ERPs reconstructed by the LDR LAE. By simply using an LAE with ERP convolutional padding, we can train an LDM to produce ERP images with the same features on either of the side borders without a border seam. This is further supported by a metric comparison in Table 2, where our approach with ERP convolutional padding performs better on all measures except for the FID score, which is only marginally worse.

## 5. Conclusion and Future Work

We have presented a novel approach to HDR environment map estimation of a scene from a single LFOV LDRI. Our approach removes the border seam artefact by implementing an ERP convolutional padding in the LAE, simultaneously improving overall metric performance. Furthermore, we have proposed a novel DiT architecture designed to better understand the ERP image format. The PanoDiT reduces the artefacts produced at the poles of the panorama and can more accurately estimate the lighting conditions than the U-Net model. This comes at an expense to the generated image quality measured by the FID score. Evaluating with standard benchmarks, we demonstrate that both of our models compete with state-of-the-art approaches whilst training on a smaller dataset than the models that perform best in terms of FID score. Future work should investigate novel ERP architecture adaptations to ultimately remove ERP distortions.



## References

- [1] Naofumi Akimoto, Seito Kasai, Masaki Hayashi, and Yoshimitsu Aoki. 360-degree image completion by two-stage conditional gans. In *2019 IEEE International Conference on Image Processing (ICIP)*, pages 4704–4708, 2019. [3](#)
- [2] Naofumi Akimoto, Yuhi Matsuo, and Yoshimitsu Aoki. Diverse plausible 360-degree image outpainting for efficient 3dcg background creation. In *Proceedings of the IEEE/CVF Conference on Computer Vision and Pattern Recognition (CVPR)*, pages 11441–11450, 2022. [1](#), [2](#), [3](#)
- [3] Jia-Xuan Bai, Jie Guo, Chenchen Wang, Zhenyu Chen, Zhen He, Shan Yang, Piaopiao Yu, Yan Zhang, and Yanwen Guo. Deep graph learning for spatially-varying indoor lighting prediction. *Science China Information Sciences*, 66:1–15, 2022. [2](#)
- [4] Shih-Hsiu Chang, Ching-Ya Chiu, Chia-Sheng Chang, Kuo-Wei Chen, Chih-Yuan Yao, Ruen-Rone Lee, and Hung-Kuo Chu. Generating 360 outdoor panorama dataset with reliable sun position estimation. In *SIGGRAPH Asia 2018 Posters*, New York, NY, USA, 2018. Association for Computing Machinery. [5](#)
- [5] Junsong Chen, Jincheng YU, Chongjian GE, Lewei Yao, Enze Xie, Zhongdao Wang, James Kwok, Ping Luo, Huchuan Lu, and Zhenguo Li. Pixart- $\alpha$ : Fast training of diffusion transformer for photorealistic text-to-image synthesis. In *The Twelfth International Conference on Learning Representations*, 2024. [1](#), [5](#)
- [6] Dachuan Cheng, Jian Shi, Yanyun Chen, Xiaoming Deng, and Xiaopeng. Zhang. Learning scene illumination by pairwise photos from rear and front mobile cameras. *Computer Graphics Forum*, 37(7):213–221, 2018. [2](#), [5](#), [6](#)
- [7] Shih-Han Chou, Wei-Lun Chao, Wei-Sheng Lai, Min Sun, and Ming-Hsuan Yang. Visual question answering on 360° images. In *Proceedings of the IEEE/CVF Winter Conference on Applications of Computer Vision (WACV)*, 2020. [3](#)
- [8] Taco Cohen, Mario Geiger, Jonas Köhler, and Max Welling. Spherical cnns. *ArXiv*, abs/1801.10130, 2018. [3](#)
- [9] Benjamin Coors, Alexandru Paul Condurache, and Andreas Geiger. Spherenet: Learning spherical representations for detection and classification in omnidirectional images. In *Proceedings of the European Conference on Computer Vision (ECCV)*, 2018. [3](#)
- [10] Mohammad Reza Karimi Dastjerdi, Jonathan Eisenmann, Yannick Hold-Geoffroy, and Jean-François Lalonde. Everlight: Indoor-outdoor editable hdr lighting estimation. In *Proceedings of the IEEE/CVF International Conference on Computer Vision (ICCV)*, pages 7420–7429, 2023. [1](#), [2](#), [3](#), [5](#), [6](#), [7](#), [4](#)
- [11] Paul Debevec. Rendering synthetic objects into real scenes: bridging traditional and image-based graphics with global illumination and high dynamic range photography. In *Proceedings of the 25th Annual Conference on Computer Graphics and Interactive Techniques*, page 189–198, New York, NY, USA, 1998. Association for Computing Machinery. [2](#)
- [12] Alexey Dosovitskiy, Lucas Beyer, Alexander Kolesnikov, Dirk Weissenborn, Xiaohua Zhai, Thomas Unterthiner, Mostafa Dehghani, Matthias Minderer, Georg Heigold, Sylvain Gelly, Jakob Uszkoreit, and Neil Houlsby. An image is worth 16x16 words: Transformers for image recognition at scale. In *International Conference on Learning Representations*, 2021. [1](#), [2](#)
- [13] Patrick Esser, Robin Rombach, and Bjorn Ommer. Taming transformers for high-resolution image synthesis. In *Proceedings of the IEEE/CVF Conference on Computer Vision and Pattern Recognition (CVPR)*, pages 12873–12883, 2021. [1](#), [2](#)
- [14] Patrick Esser, Sumith Kulal, Andreas Blattmann, Rahim Entezari, Jonas Müller, Harry Saini, Yam Levi, Dominik Lorenz, Axel Sauer, Frederic Boesel, Dustin Podell, Tim Dockhorn, Zion English, and Robin Rombach. Scaling rectified flow transformers for high-resolution image synthesis. In *Proceedings of the 41st International Conference on Machine Learning*, pages 12606–12633. PMLR, 2024. [1](#), [4](#), [5](#)
- [15] Qi Feng, Hubert P. H. Shum, and Shigeo Morishima. 360 depth estimation in the wild - the depth360 dataset and the segfuse network. In *2022 IEEE Conference on Virtual Reality and 3D User Interfaces (VR)*, pages 664–673, 2022. [3](#)
- [16] Marc-André Gardner, Kalyan Sunkavalli, Ersin Yumer, Xiaohui Shen, Emiliano Gambaretto, Christian Gagné, and Jean-François Lalonde. Learning to predict indoor illumination from a single image. *ACM Transactions on Graphics (SIGGRAPH Asia)*, 9(4), 2017. [1](#), [2](#), [5](#)
- [17] Marc-Andre Gardner, Yannick Hold-Geoffroy, Kalyan Sunkavalli, Christian Gagne, and Jean-Francois Lalonde. Deep parametric indoor lighting estimation. In *Proceedings of the IEEE/CVF International Conference on Computer Vision (ICCV)*, 2019. [1](#), [2](#)
- [18] Mathieu Garon, Kalyan Sunkavalli, Sunil Hadap, Nathan Carr, and Jean-François Lalonde. Fast spatially-varying indoor lighting estimation. In *2019 IEEE/CVF Conference on Computer Vision and Pattern Recognition (CVPR)*, pages 6901–6910, 2019. [1](#), [2](#)
- [19] Vasileios Gkitsas, Nikolaos Zioulis, Federico Alvarez,

- Dimitrios Zarpalas, and Petros Daras. Deep lighting environment map estimation from spherical panoramas. In *Proceedings of the IEEE/CVF Conference on Computer Vision and Pattern Recognition (CVPR) Workshops*, 2020. 2
- [20] Manu Gond, Emin Zerman, Sebastian Knorr, and Mårten Sjöström. LFSphereNet: Real time spherical light field reconstruction from a single omnidirectional image. In *ACM SIGGRAPH European Conference on Visual Media Production (CVMP)*, 2023. 3
- [21] Takayuki Hara, Yusuke Mukuta, and Tatsuya Harada. Spherical image generation from a single image by considering scene symmetry. *Proceedings of the AAAI Conference on Artificial Intelligence*, 35(2): 1513–1521, 2021. 3
- [22] Jack Hilliard, Adrian Hilton, and Jean-Yves Guillemaut. 360u-former: Hdr illumination estimation with panoramic adapted vision transformers. In *European Conference on Computer Vision (ECCV) Workshops*, 2024. 2, 3, 5, 6, 7, 1, 4
- [23] Jack Oliver Hilliard, Adrian Hilton, and Jean-Yves Guillemaut. Hdr illumination outpainting with a two-stage gan model. In *Proceedings of the 20th ACM SIGGRAPH European Conference on Visual Media Production*, New York, NY, USA, 2023. Association for Computing Machinery. 2, 3
- [24] Yannick Hold-Geoffroy, Kalyan Sunkavalli, Sunil Hadap, Emiliano Gambaretto, and Jean-Francois Lalonde. Deep outdoor illumination estimation. In *Proceedings of the IEEE Conference on Computer Vision and Pattern Recognition (CVPR)*, 2017. 2
- [25] Yannick Hold-Geoffroy, Akshaya Athawale, and Jean-Francois Lalonde. Deep sky modeling for single image outdoor lighting estimation. In *Proceedings of the IEEE/CVF Conference on Computer Vision and Pattern Recognition (CVPR)*, 2019. 2
- [26] Mohammad Reza Karimi Dastjerdi, Yannick Hold-Geoffroy, Jonathan Eisenmann, Siavash Khodadadeh, and Jean-François Lalonde. Guided co-modulated GAN for 360° field of view extrapolation. *International Conference on 3D Vision (3DV)*, 2022. 1, 2, 3, 6
- [27] Tero Karras, Samuli Laine, Miika Aittala, Janne Hellsten, Jaakko Lehtinen, and Timo Aila. Analyzing and improving the image quality of stylegan. In *Proceedings of the IEEE/CVF Conference on Computer Vision and Pattern Recognition (CVPR)*, 2020. 1, 2
- [28] Kyunghun Kim, Yeohun Yun, Keon-Woo Kang, Kyeongbo Kong, Siyeong Lee, and Suk-Ju Kang. Painting outside as inside: Edge guided image outpainting via bidirectional rearrangement with progressive step learning. In *2021 IEEE Winter Conference on Applications of Computer Vision (WACV)*, pages 2121–2129, 2021. 3
- [29] Mengtian Li, Jie Guo, Xiufen Cui, Rui Pan, Yanwen Guo, Chenchen Wang, Piaopiao Yu, and Fei Pan. Deep spherical gaussian illumination estimation for indoor scene. In *Proceedings of the 1st ACM International Conference on Multimedia in Asia*, New York, NY, USA, 2020. Association for Computing Machinery. 2
- [30] Wenbo Li, Xin Yu, Kun Zhou, Yibing Song, and Zhe Lin. Image inpainting via iteratively decoupled probabilistic modeling. In *The Twelfth International Conference on Learning Representations*, 2024. 1, 2, 3
- [31] Zhixin Ling, Zhen Xing, Xiangdong Zhou, Manliang Cao, and Guichun Zhou. Panoswin: A pano-style swin transformer for panorama understanding. In *Proceedings of the IEEE/CVF Conference on Computer Vision and Pattern Recognition (CVPR)*, pages 17755–17764, 2023. 2, 3, 5
- [32] Zhuqiang Lu, Kun Hu, Chaoyue Wang, Lei Bai, and Zhiyong Wang. Autoregressive omni-aware outpainting for open-vocabulary 360-degree image generation. *Proceedings of the AAAI Conference on Artificial Intelligence*, 38(13):14211–14219, 2024. 1, 2
- [33] Andreas Lugmayr, Martin Danelljan, Andres Romero, Fisher Yu, Radu Timofte, and Luc Van Gool. Repaint: Inpainting using denoising diffusion probabilistic models. In *Proceedings of the IEEE/CVF Conference on Computer Vision and Pattern Recognition (CVPR)*, pages 11461–11471, 2022. 1, 2
- [34] William Peebles and Saining Xie. Scalable diffusion models with transformers. In *Proceedings of the IEEE/CVF International Conference on Computer Vision (ICCV)*, pages 4195–4205, 2023. 5
- [35] Ethan Perez, Florian Strub, Harm de Vries, Vincent Dumoulin, and Aaron Courville. Film: Visual reasoning with a general conditioning layer. *Proceedings of the AAAI Conference on Artificial Intelligence*, 32(1), 2018. 5
- [36] Dustin Podell, Zion English, Kyle Lacey, Andreas Blattmann, Tim Dockhorn, Jonas Müller, Joe Penna, and Robin Rombach. SDXL: Improving latent diffusion models for high-resolution image synthesis. In *The Twelfth International Conference on Learning Representations*, 2024. 1, 2, 3
- [37] Robin Rombach, Andreas Blattmann, Dominik Lorenz, Patrick Esser, and Björn Ommer. High-resolution image synthesis with latent diffusion models. In *Proceedings of the IEEE/CVF Conference on Computer Vision and Pattern Recognition (CVPR)*, pages 10684–10695, 2022. 1, 2, 3, 5
- [38] Axel Sauer, Dominik Lorenz, Andreas Blattmann, and Robin Rombach. Adversarial diffusion distillation. In



- Computer Vision – ECCV 2024*, pages 87–103, Cham, 2025. Springer Nature Switzerland. 1, 2, 3
- [39] Zhijie Shen, Chunyu Lin, Kang Liao, Lang Nie, Zishuo Zheng, and Yao Zhao. Panoformer: Panorama transformer for indoor 360° depth estimation. In *European Conference on Computer Vision*, pages 195–211. Springer, 2022. 3
- [40] Gowri Somanath and Daniel Kurz. Hdr environment map estimation for real-time augmented reality. In *Proceedings of the IEEE/CVF Conference on Computer Vision and Pattern Recognition (CVPR)*, pages 11298–11306, 2021. 1, 2, 3
- [41] Shuran Song and Thomas Funkhouser. Neural illumination: Lighting prediction for indoor environments. In *Proceedings of the IEEE/CVF Conference on Computer Vision and Pattern Recognition (CVPR)*, 2019. 1, 2
- [42] Pratul P. Srinivasan, Ben Mildenhall, Matthew Tancik, Jonathan T. Barron, Richard Tucker, and Noah Snavely. Lighthouse: Predicting lighting volumes for spatially-coherent illumination. In *Proceedings of the IEEE/CVF Conference on Computer Vision and Pattern Recognition (CVPR)*, 2020. 1, 2
- [43] Yu-Chuan Su and Kristen Grauman. Learning spherical convolution for fast features from 360° imagery. In *Advances in Neural Information Processing Systems*. Curran Associates, Inc., 2017. 3
- [44] Yu-Chuan Su and Kristen Grauman. Kernel transformer networks for compact spherical convolution. In *Proceedings of the IEEE/CVF Conference on Computer Vision and Pattern Recognition (CVPR)*, 2019. 3
- [45] Yu-Chuan Su and Kristen Grauman. Learning spherical convolution for 360° recognition. *IEEE Transactions on Pattern Analysis and Machine Intelligence*, 44(11):8371–8386, 2022. 3
- [46] Guangcong Wang, Yinuo Yang, Chen Change Loy, and Ziwei Liu. Stylelight: Hdr panorama generation for lighting estimation and editing. In *European Conference on Computer Vision (ECCV)*, 2022. 1, 2
- [47] Hai Wang, Xiaoyu Xiang, Yuchen Fan, and Jing-Hao Xue. Customizing 360-degree panoramas through text-to-image diffusion models. In *Proceedings of the IEEE/CVF Winter Conference on Applications of Computer Vision (WACV)*, pages 4933–4943, 2024. 1, 2, 3
- [48] Ting-Chun Wang, Ming-Yu Liu, Jun-Yan Zhu, Andrew Tao, Jan Kautz, and Bryan Catanzaro. High-resolution image synthesis and semantic manipulation with conditional gans. In *2018 IEEE/CVF Conference on Computer Vision and Pattern Recognition*, pages 8798–8807, 2018. 1
- [49] Zhendong Wang, Xiaodong Cun, Jianmin Bao, Wengang Zhou, Jianzhuang Liu, and Houqiang Li. Uformer: A general u-shaped transformer for image restoration. In *Proceedings of the IEEE/CVF Conference on Computer Vision and Pattern Recognition (CVPR)*, pages 17683–17693, 2022. 1, 2, 3
- [50] Henrique Weber, Mathieu Garon, and Jean-François Lalonde. Editable indoor lighting estimation. In *European Conference on Computer Vision (ECCV)*, 2022. 1, 2, 5, 6, 7, 3, 4
- [51] Olivia Wiles, Georgia Gkioxari, Richard Szeliski, and Justin Johnson. Synsin: End-to-end view synthesis from a single image. In *Proceedings of the IEEE/CVF Conference on Computer Vision and Pattern Recognition (CVPR)*, 2020. 1
- [52] Tianhao Wu, Chuanxia Zheng, and Tat-Jen Cham. Panodiffusion: 360-degree panorama outpainting via diffusion. In *The Twelfth International Conference on Learning Representations*, 2024. 1, 2, 3
- [53] Shaoan Xie, Zhifei Zhang, Zhe Lin, Tobias Hinz, and Kun Zhang. Smartbrush: Text and shape guided object inpainting with diffusion model. In *Proceedings of the IEEE/CVF Conference on Computer Vision and Pattern Recognition (CVPR)*, pages 22428–22437, 2023. 1, 2
- [54] Heeseung Yun, Sehun Lee, and Gunhee Kim. Panoramic vision transformer for saliency detection in 360 videos. In *Computer Vision – ECCV 2022: 17th European Conference, Tel Aviv, Israel, October 23–27, 2022, Proceedings, Part XXXV*, page 422–439, Berlin, Heidelberg, 2022. Springer-Verlag. 3
- [55] Fangneng Zhan, Changgong Zhang, Wenbo Hu, Shijian Lu, Feiying Ma, Xuansong Xie, and Ling Shao. Sparse needlets for lighting estimation with spherical transport loss. In *Proceedings of the IEEE/CVF International Conference on Computer Vision (ICCV)*, pages 12830–12839, 2021. 2
- [56] Fangneng Zhan, Changgong Zhang, Yingchen Yu, Yuan Chang, Shijian Lu, Feiying Ma, and Xuansong Xie. Emilight: Lighting estimation via spherical distribution approximation. In *Proceedings of the AAAI Conference on Artificial Intelligence*, 2021. 3, 6, 2
- [57] Fangneng Zhan, Yingchen Yu, Changgong Zhang, Rongliang Wu, Wenbo Hu, Shijian Lu, Feiying Ma, Xuansong Xie, and Ling Shao. Gmlight: Lighting estimation via geometric distribution approximation. *IEEE Transactions on Image Processing*, 31:2268–2278, 2022. 2
- [58] Jinsong Zhang and Jean-Francois Lalonde. Learning high dynamic range from outdoor panoramas. In *Proceedings of the IEEE International Conference on Computer Vision (ICCV)*, 2017. 1, 2

- [59] Jinsong Zhang, Kalyan Sunkavalli, Yannick Hold-Geoffroy, Sunil Hadap, Jonathan Eisenman, and Jean-Francois Lalonde. All-weather deep outdoor lighting estimation. In *Proceedings of the IEEE/CVF Conference on Computer Vision and Pattern Recognition (CVPR)*, 2019. [2](#)
- [60] Shengyu Zhao, Jonathan Cui, Yilun Sheng, Yue Dong, Xiao Liang, Eric I Chang, and Yan Xu. Large scale image completion via co-modulated generative adversarial networks. In *International Conference on Learning Representations (ICLR)*, 2021. [1](#), [2](#)
- [61] Jia Zheng, Junfei Zhang, Jing Li, Rui Tang, Shenghua Gao, and Zihan Zhou. Structured3d: A large photo-realistic dataset for structured 3d modeling. In *Proceedings of The European Conference on Computer Vision (ECCV)*, 2020. [5](#)

# HDR Environment Map Estimation with Latent Diffusion Models

## Supplementary Material

### 6. Additional Quantitative Results

Table 3 contains an extensive comparison with illumination estimation methods. Two versions of [17] are compared: the original (3) where 3 light sources are estimated, and a version (1) trained to predict a single parametric light. We also compare to Lighthouse [42], which expects a stereo pair as input, instead a second image is generated with a small baseline using [51] (visual inspection confirmed this yields results comparable to the published work). For [18], the coordinates of the image centre are selected for the object position. For [40], the proposed “Cluster ID loss”, and tonemapping are used with a pix2pixHD [48] network architecture.

### 7. Additional Qualitative Results

In Figure 8, we provide additional environment maps for both indoor and outdoor scenes from both of our models to compare with Weber’22 [50], EverLight [10] and 360U-Former [22]. Additionally, we render three spheres of different surface materials: diffuse, mirror-reflective and specular. This visualises how objects will appear when rendered by the environment maps and helps to assess estimated lighting accuracy against the state-of-the-art methods. The rendered spheres are presented alongside the generated environment maps in Figure 9. When observing the rendered spheres of indoor scenes with our models, we observe colours similar to the ground-truth renders. However, in a few examples, light sources are out of place. For outdoor scenes, our models consistently and correctly estimate the sun position and the amount of cloud cover. These results reflect the quantitative results in Table 3.

Method	si-RMSE↓	RMSE↓	RGB ang.↓	PSNR↑	FID↓
INDOOR METHODS					
Ours <sub>U-Net</sub>	0.048	<u>0.091</u>	11.13°	<u>12.98</u>	<u>64.31</u>
OursPanoDiT	<u>0.046</u>	<b>0.085</b>	10.78°	<b>13.49</b>	83.49
360U-Former[22]	<b>0.033</b>	0.110	6.11°	11.68	119.91
Hilliard’23[23]	0.112	0.300	6.50°	10.05	158.60
EverLight[10]	0.087	0.239	5.75°	10.04	65.50
Weber’22[50]	0.079	0.196	<u>4.08°</u>	12.95	130.13
StyleLight[46]	0.130	0.261	7.05°	12.85	121.60
Gardner’19(1)[17]	0.099	0.229	4.42°	12.21	410.12
Gardner’19(3)[17]	0.105	0.507	4.59°	10.90	386.43
Gardner’17[16]	0.123	0.628	8.29°	10.22	253.40
Garon’19[18]	0.096	0.255	8.06°	9.73	324.51
Lighthouse[42]	0.121	0.254	4.56°	9.81	174.52
EMLight[56]	0.099	0.232	<b>3.99°</b>	10.34	135.97
EnvmapNet[40]	0.097	0.286	7.67°	11.74	221.85
ImmerseGAN[26]	0.091	0.215	7.89°	10.87	<b>55.46</b>
OUTDOOR METHODS					
Ours <sub>U-Net</sub>	<u>0.052</u>	0.152	<u>5.44°</u>	11.23	83.17
OursPanoDiT	<u>0.052</u>	<b>0.135</b>	5.62°	<u>12.44</u>	90.74
360U-Former[22]	<b>0.049</b>	0.161	<b>4.00°</b>	<b>13.27</b>	102.63
EverLight[10]	0.162	0.385	8.30°	11.01	<u>61.49</u>
ImmerseGAN[26]	0.175	0.341	9.56°	10.91	<b>34.43</b>
Zhang ’19[59]	0.225	1.058	11.80°	10.91	449.49

Table 3. Indoor and outdoor quantitative comparison with various illumination estimation methods. The metrics si-RMSE, RMSE, RGB ang. and PSNR are evaluated by rendering a diffuse scene. The FID score is calculated on the generated environment maps. The **best** and second-best scores for each metric and domain are highlighted.



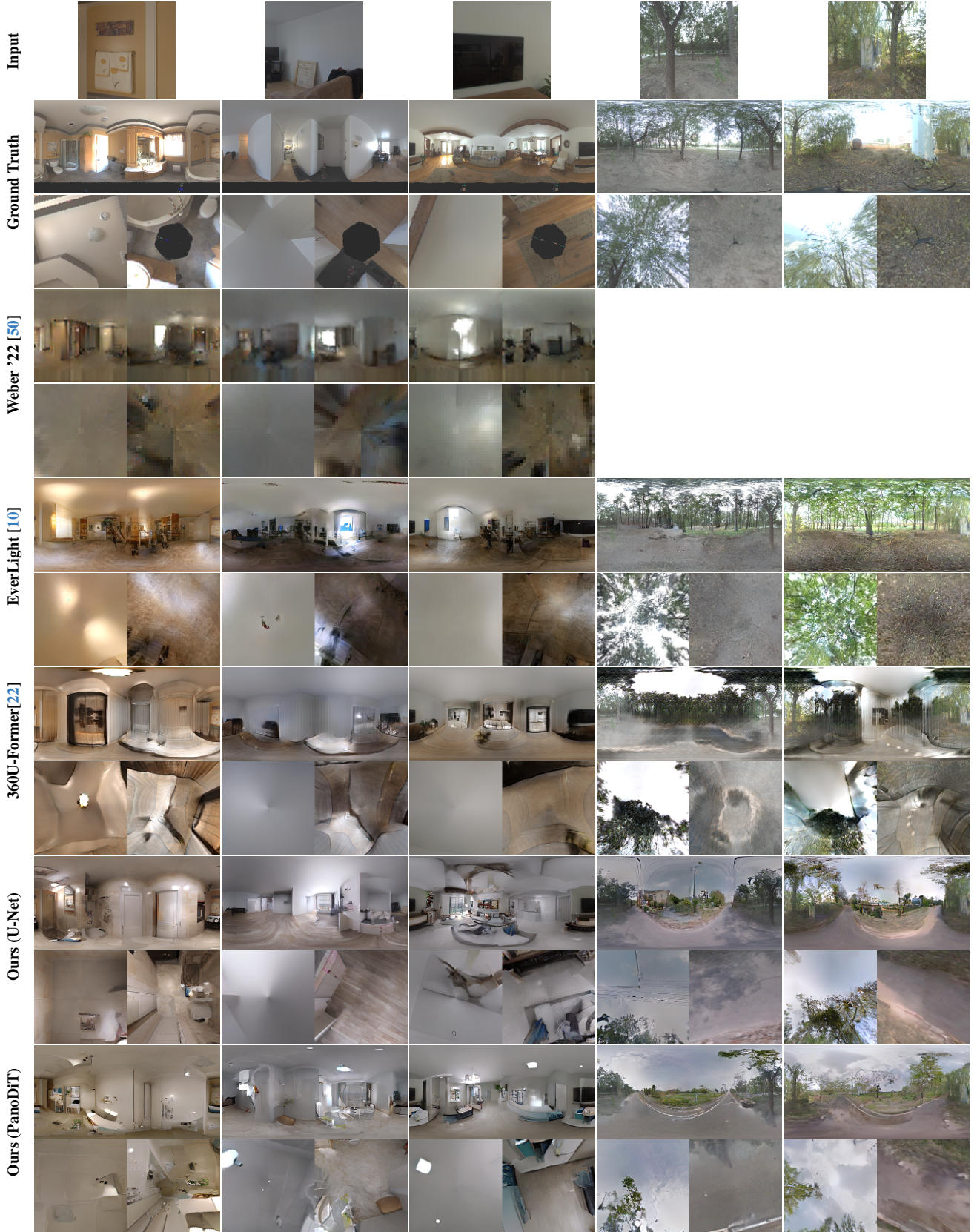


Figure 8. Indoor qualitative comparison of our method with state-of-the-art methods. For each method and input LFOV image, we show the ERP rotated 180°, to show potential border seams, and the top and bottom cube map faces, to visualise generation at the poles.



